Journal of Materials Chemistry C

ROYAL SOCIETY OF CHEMISTRY

PAPER

View Article Online
View Journal | View Issue

Cite this: J. Mater. Chem. C, 2024, 12, 6177

Efficient orange organic light-emitting diodes employing a central aniline bridged multiresonant thermally activated delayed fluorescence emitter†

Sen Wu,‡[a] Ya-Nan Hu,‡[b] Jingxiang Wang,[a] Dianming Sun,*[a] Kai Wang,[b] Xiao-Hong Zhang *[bc] and Eli Zysman-Colman *[a]

Received 5th February 2024,
Accepted 29th March 2024

DOI: 10.1039/d4tc00506f

rsc.li/materials-c

Multiresonant thermally activated delayed fluorescence (MR-TADF) compounds are attractive for use in organic light-emitting diodes as they show narrowband emission, are bright, and can harvest both singlet and triplet excitons for the emission of light. Reflected in the paucity of examples of orange-to-red emitters, developing MR-TADF emitters that emit beyond the green remains an outstanding materials design challenge. In this work, we report one of the first carbonyl-based orange MR-TADF emitters, **DDiKTa-A**, which is based on the dimerization of the sky-blue emitting **DiKTa** through a central aniline bridge. **DDiKTa-A** emits at λ_{PL} of 562 nm and has high photoluminescence quantum yield of 92% in 2 wt% doped films in mCP. **DDiKTa-A** exhibits temperature dependent steady-state photoluminescence in 2-MeTHF, acting as an indirect indicator of the polarity of the medium. The OLEDs with **DDiKTa-A** showed an EQE_{max} of 20.3%, but with significant efficiency roll-off (EQE_{100} of 13.2%). The EQE_{max} was improved, and the efficiency roll-off mitigated by incorporating an assistant dopant, 4CzIPN, within the emissive layer of the device. The hyperfluorescence device showed an EQE_{max} of 24.3%, which decreased to 22.5 and 14.6% at 100 and 1000 cd m^{-2}, respectively.

Introduction

Multiresonant thermally activated delayed fluorescence (MR-TADF) materials show significant potential as emitters in organic light-emitting diodes (OLEDs) as they have the requisite narrowband emission to produce the required saturated colors for high-definition displays.[1–5] Unlike conventional donor–acceptor (D–A) TADF emitters, the structural rigidity inherent in most MR-TADF emitters reduces geometric relaxation upon excitation, resulting in a narrowband emission. The disposition of electron-rich and electron-deficient groups within the polycyclic aromatic hydrocarbon skeleton produces an emissive excited state of short-range charge-transfer (SRCT) character where there is a small exchange integral reflected in the moderately small singlet–triplet energy gap, ΔE_{ST}, that enables TADF.

To date, numerous MR-TADF emitters have been developed, some of which produce OLEDs that show fantastic performance including examples where the maximum external quantum efficiency (EQE_{max}) exceeds 40%.[6] There are now many reported blue and green MR-TADF OLEDs including examples that approach the B.T. 2020 industry standard for green[7–11] and blue emission.[12–15] However, examples of orange/red MR-TADF OLEDs remain relatively rare due to the challenges in emitter design to red-shift the emission of the emitters.[6] There are currently two primary methods for shifting the emission to the red: (1) Enhancing the donor and acceptor strength by constructing systems with electron-accepting (A) and donating atoms (D) in A-*para*-A and D-*para*-D regiochemistry;[16–19] (2) Decorating the MR-TADF core with donor or acceptor substituents to tune the energy of the emissive core;[20,21] note that the use of too strong donors or acceptors results in the excited state being of long-range charge transfer (LRCT) character, resulting in less bright and broader emission. Dimerization of MR-TADF emitters is a distinct strategy for realizing red-shifted emission *via* extending the conjugation area. To date, there are only limited samples that have been reported based on this latter strategy.[22–24] Our group reported the first example of a dimeric MR-TADF emitter by connecting two **DiKTa** units (aka QAO or QAD)[25–27] through a single bond in **DDiKTa** (Scheme S1, ESI†).[22] The photoluminescence

[a] Organic Semiconductor Centre, EaStCHEM School of Chemistry, University of St Andrews, St Andrews, Fife KY16 9ST, UK. E-mail: eli.zysman-colman@st-andrews.ac.uk, sd235@st-andrews.ac.uk; Fax: +44-1334 463808; Tel: +44-1334 463826
[b] Institute of Functional Nano & Soft Materials (FUNSOM), Joint International Research Laboratory of Carbon-Based Functional Materials and Devices, Soochow University, Suzhou, Jiangsu 215123, P. R. China. E-mail: xiaohong_zhang@suda.edu.cn
[c] Jiangsu Key Laboratory of Advanced Negative Carbon Technologies, Soochow University, Suzhou, 215123, Jiangsu, P. R. China

† Electronic supplementary information (ESI) available: ^{1}H and ^{13}C-NMR spectra, HRMS, EA of the target compounds; supplementary computational, photophysical and device data. See DOI: https://doi.org/10.1039/d4tc00506f

‡ Equal contributions.

(PL) was observed to red-shift from 451 nm for **DiKTa** to 470 nm for **DDiKTa** in toluene. Yasuda and co-workers reported another two isomeric MR-TADF dimers formed by tethering two MR-TADF fragments with different regiochemistry, *para*-B-π-B for ***p*-CzB** and *para*-N-π-N for ***m*-CzB**, as shown in Scheme S1 (ESI†).[23] Compared to **DtBuCzB** (λ_{PL} = 489 nm), ***p*-CzB** and ***m*-CzB** emit at 504 and 515 nm in toluene, representing a modest red-shift of their PL.[28] The devices with ***p*-CzB** and ***m*-CzB** showed EQE_{max} of 20.2 and 23.5%, respectively. Lan and co-workers reported another two MR-TADF dimeric emitters, **DBF-DBN** and **DBT-DBN** (Scheme S1, ESI†).[24] The OLEDs with **DBF-DBN** and **DBT-DBN** emitted at 514 and 516 nm and showed EQE_{max} of 21.5 and 31.3%, respectively. Each of these three reports documents a red-shifted emission of the dimeric emitters compared to their monomeric counterparts; however, the emission is in the green region and no example to date demonstrates that this strategy can be used to push the emission further to the red.

Here, we report the emitter **DDiKTa-A**, a compound that contains two **DiKTa** units bridged by a central aniline (Fig. 1). Using this design based on a synergy between a compound containing *para*-N-π-N conjugation and two emissive luminophores leads to a strong red-shift of the emission from blue (λ_{PL} = 453 nm) for **DiKTa**[29] to yellow (λ_{PL} = 551 nm) for **DDiKTa-A** in toluene solution. The emission of **DDiKTa-A** shows a significant temperature sensitivity in 2-MeTHF, reflected in a color change from 566 to 638 nm across a temperature range from 123 to 298 K. In 2 wt% doped films in 1,3-bis(*N*-carbazolyl)benzene (mCP), **DDiKTa-A** emits at 562 nm, has a high photoluminescence quantum yield, Φ_{PL}, of 92%, and a delayed lifetime, τ_d, of 279 μs. The OLEDs with **DDiKTa-A** showed an EQE_{max} of 20.3% at λ_{EL} of 573 nm but with a severe efficiency roll-off (EQE_{100} of 13.2%). To tackle the observed efficiency roll-off, hyperfluorescence (HF) devices incorporating 4CzIPN as the assistant dopant were fabricated and showed much improved performance, with an enhanced EQE_{max} of 24.3% and a reduced efficiency roll-off with EQE_{100} of 22.5% and EQE_{1000} of 14.6% at λ_{EL} of 574 nm.

Results and discussion

DDiKTa-A was obtained in one step from **DiKTa-Br**[22] *via* a two-fold palladium-catalysed Buchwald-Hartwig cross-coupling reaction with 4-*tert*-butylaniline (Scheme S1, ESI†). **DDiKTa-A** was purified by column chromatography and then by gradient-temperature vacuum sublimation. The identity and purity of **DDiKTa-A** was assessed using a combination of ^{1}H & ^{13}C nuclear magnetic resonance spectroscopy, high-resolution mass spectrometry, melting point determination, high-pressure liquid chromatography and elemental analysis (Fig. S1–S5, ESI†).

The optoelectronic properties of **DDiKTa-A** were firstly modelled using a combination of density functional theory (DFT) and wavefunction-based methods as the latter have been previously shown to accurately predict the excited state energies of MR-TADF compounds, including the structurally related **DiDOBNA-N**.[15,30] The geometry in the ground state and the HOMO/LUMO levels were calculated at the PBE0/6-31G(d,p) level. As shown in Fig. 2a, the LUMO is mostly localized on the **DiKTa** moieties, while the HOMO is delocalized across the whole molecule. Compared to the HOMO/LUMO levels of **DiKTa** (−6.20/−2.23 eV)[31] and **DDiKTa** (−6.04/−2.34) the HOMO of **DDiKTa-A** is significantly destabilized while the LUMO is effectively unchanged (−5.39/−2.24 eV). The resulting energy gap (ΔE) of 3.15 eV is smaller than those of **DiKTa** (3.97 eV) and **DDiKTa** (3.70 eV).[32] As a result of the amine, there is considerable conformational flexibility in **DDiKTa-A**, reflected in the differences in geometry between the ground

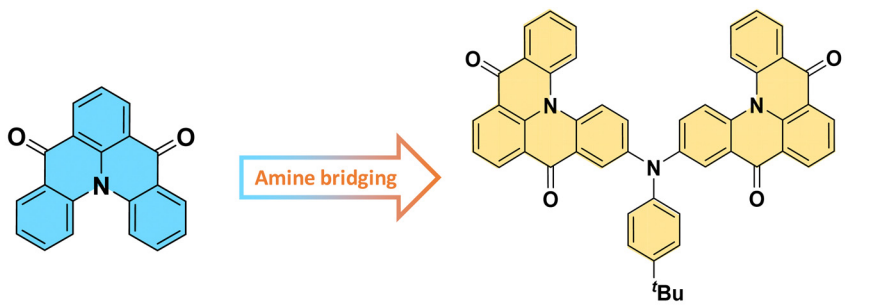

DiKTa

λ_{PL} = 463 nm, Φ_{PL} = 75%, ΔE_{ST} =0.20 eV
in 3.5 wt% mCP film
λ_{EL} = 465 nm; EQE_{max} = 14.7%,
EQE_{1000} = 3.3% (OLED)
Adv. Optical. Mater., **2020**, *8*, 1901627

DDiKTa-A

λ_{PL} = 562 nm, Φ_{PL} = 92%, ΔE_{ST} = 0.16 eV
in 2 wt% mCP film
λ_{EL} = 572 nm; EQE_{max} = 20.3%,
EQE_{1000} = 3.9% (OLED)
λ_{EL} = 574 nm; EQE_{max} = 24.3%,
EQE_{1000} = 14.6% (HF-OLED)
This work

Fig. 1 Chemical structures, photophysical and device properties of **DiKTa** and **DDiKTa-A**.

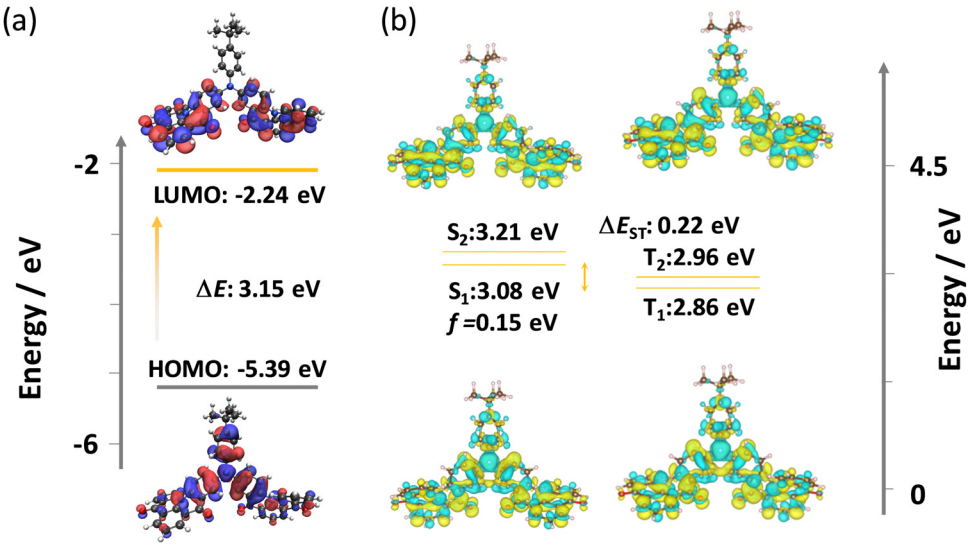

Fig. 2 (a) Distributions of the frontier molecular orbitals (isovalue: 0.02) of **DDiKTa-A**, calculated in the gas phase at the PBE0/6-31G(d,p) level; (b) difference density plots (isovalue: 0.001) of S_1/S_2 and T_1/T_2 excited states (calculated in the gas phase at the SCS-ADC(2)/cc-pVDZ level) for **DDiKTa-A**. *f* is the oscillator strength.

and singlet excited state (RMSD value of 0.2757, Fig. S6, ESI†), which will likely lead to a broad emission similar to that observed for **DiDOBNA-N**.[15] The energies of the low-lying singlet and triplet excited states were calculated at the SCS-ADC(2)/cc-pVDZ level (Fig. S2b, ESI†).[33,34] The difference density plots reveal the expected alternating pattern of increasing and decreasing electron density in the excited states as compared to the ground state, reflective of states of SRCT character. The plots also show that the electron density is delocalized across both DiKTa moieties and the bridging nitrogen atom. The distribution pattern for the S_2/T_2 is similar to that of the S_1/T_1 states but does not involve as significantly the bridging aniline. The S_1 energy level is 3.08 eV, which is stabilized compared to that of **DDiKTa** of 3.39 eV and **DiKTa** of 3.46 eV, indicating that the emission should be lower in energy. The calculated ΔE_{ST} of 0.22 eV is smaller than the predicted value of 0.27 eV for both **DiKTa** and **DDiKTa**. The SOC matrix element (SOCME) between S_1 and T_1 at the T_1-optimized geometry (Fig. S7, ESI†) was calculated to be 0.49 cm^{-1} while that from T_2 to S_1 was 0.44 cm^{-1} (Fig. S8, ESI†).

The electrochemical properties were investigated using cyclic voltammetry (CV) and differential pulse voltammetry (DPV) in dichloromethane (Fig. S10, ESI†). The CV of **DDiKTa-A** shows reversible oxidation and reduction waves. The oxidation (E_{ox}) and reduction potentials (E_{red}), determined from the respective peaks in the DPV, are 0.98 and −1.32 eV *versus* a saturated calomel electrode (SCE). The corresponding HOMO and LUMO levels are calculated to be −5.32 and −3.02 eV. The HOMO is

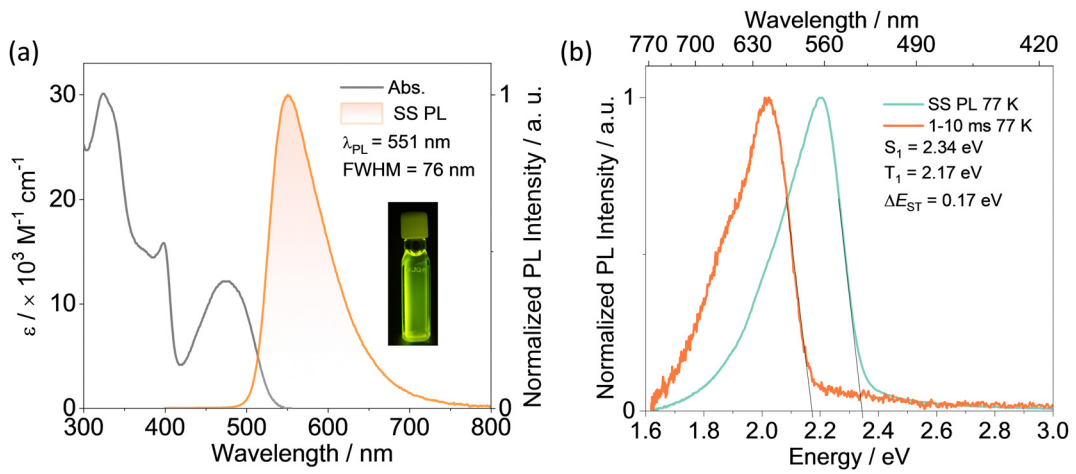

Fig. 3 (a) Absorption and steady-state photoluminescence (SS PL) spectra in toluene at RT, λ_{exc} = 340 nm. (Inset: photo of **DDiKTa-A** in toluene and irradiated with a UV torch, λ_{exc} = 365 nm.) (b) The SS PL and phosphorescence spectra (1–10 ms in 2-MeTHF glass at 77 K), λ_{exc} = 340 nm.

destabilized while the LUMO is of similar energy to those of **DiKTa** (−6.12 eV/−3.00 eV),[29] reflecting the predictions from DFT.

The UV-vis absorption spectrum of **DDiKTa-A** in dilute toluene solution (10^{-5} M) at room temperature is shown in Fig. 3a. There are three identifiable absorption bands with peaks of 323, 397 and 473 nm, which generally match with the simulated absorption spectra (Fig. S9, ESI†). The two intense, higher energy bands (ε of 3.0×10^4 and 1.6×10^4 M^{-1} cm^{-1}, respectively) are associated, respectively, with π–π^* transitions across the **DiKTa** backbone (λ_{abs} = 334 nm, $\varepsilon = 3.5 \times 10^3$ M^{-1} cm^{-1})[25] and the whole skeleton, based on an analysis of the TDA-DFT calculations (Fig. S9, ESI†). The absorption band at 474 nm ($\varepsilon = 1.2 \times 10^4$ M^{-1} cm^{-1}) is associated with the characteristic SRCT state and is both red-shifted and weaker compared to the SRCT band of **DiKTa** (λ_{abs} = 435 nm with $\varepsilon = 2.1 \times 10^4$ M^{-1} cm^{-1}), likely implicating that this state in **DDiKTa-A** contains an admixture of SRCT and LRCT character.[25] The steady-state photoluminescence (PL) spectrum in toluene of **DDiKTa-A** is broad, having a peak at λ_{PL} of 551 nm and a FWHM of 76 nm. This emission is significantly red-shifted and broader compared to that of **DDiKTa** (λ_{PL} = 470 nm, FWHM = 47 nm), of **DiKTa** (λ_{PL} = 453 nm, FWHM = 27 nm), and of **DiDOBNA-N** (λ_{PL} = 426 nm, FWHM = 43 nm).[25,32] The broader emission is attributed to combination of an emissive excited state possessing an admixture of SRCT and LRCT character and a conformationally flexible structure. Distinct from that observed for these three compounds, there is a more significant positive solvatochromism (Fig. S11, ESI†) that is consistent with of an emissive excited state that possesses mixed SRCT and LRCT character.

The energies of the S_1 and T_1 states were determined from the onsets of the steady-state photoluminescence (SS PL) spectra and delayed emission in 2-MeTHF glass at 77 K (Fig. 3b). The extracted S_1 and T_1 energies are 2.34 and 2.17 eV, respectively, leading to a ΔE_{ST} of 0.17 eV, which is smaller than that of **DiKTa** (0.20 eV), **DDiKTa** (0.21 eV), and **DIDOBNA-N** (0.22 eV). The time-resolved PL (TR PL) decays in toluene are shown in Fig. S12b (ESI†). The emission decays with biexponential kinetics, with prompt lifetime, τ_p, of 16.3 ns and delayed lifetime, τ_d, of 41.0 μs under N_2; the delayed emission was quenched upon exposure to air (Fig. S12a, ESI†). The Φ_{PL} decreases from 44 to 36% upon exposure to air. The inferred kinetics rate constants are summarized in Table S2 (ESI†) and the rate constant for RISC, k_{RISC}, is 1.63×10^4 s^{-1}. Notably, no delayed lifetime in toluene solution was observed for **DiKTa**, **DDiKTa**, and **DIDOBNA-N**.

As shown in Fig. 4, the SS PL of **DDiKTa-A** exhibits a temperature dependence in 2-MeTHF solution (123–298 K). **DDiKTa-A** shows a structureless orange emission at 577 nm at RT and when the temperature decreases to 163 K there is a gradual red-shift of the emission to 638 nm. This phenomenon can be attributed to the increased dielectric constant of 2-MeTHF upon cooling, which stabilizes the LRCT state of **DDiKTa-A**.[35–37] When the temperature is close to the glass transition temperature of 2-MeTHF (131–142 K)[38] the emission

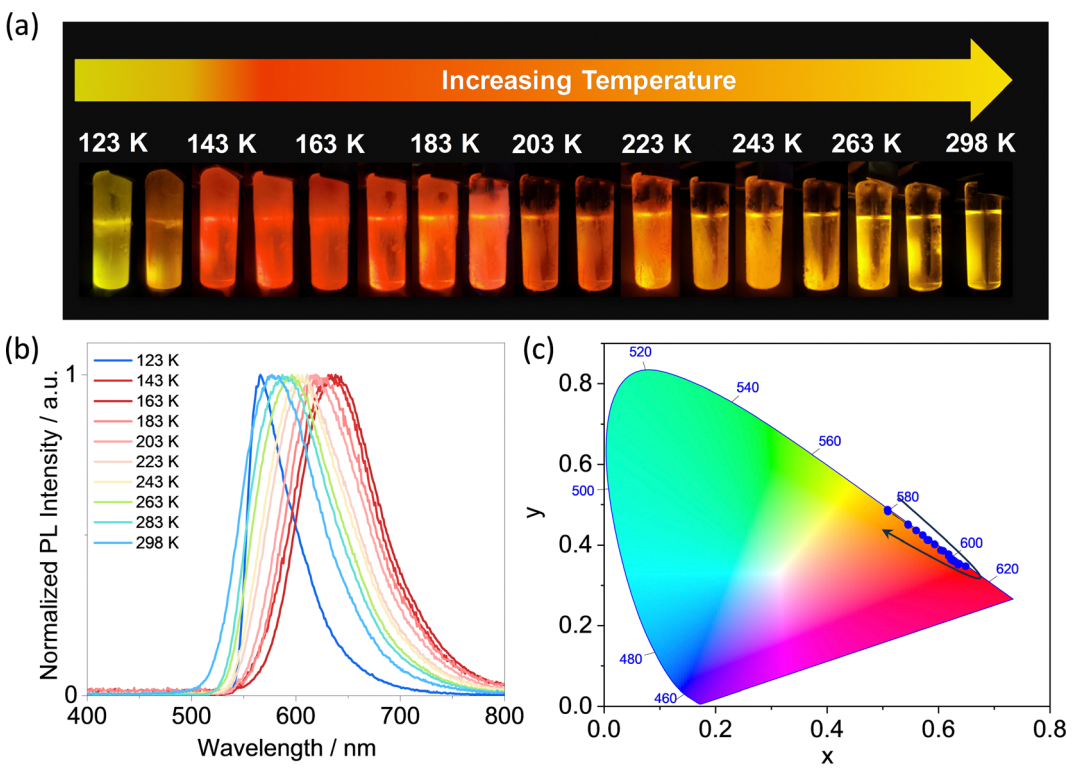

Fig. 4 (a) Images showing samples in 2-MeTHF irradiated with a UV torch at different temperatures. (b) Temperature-dependent steady-state PL spectra in 2-MeTHF, λ_{exc} = 365 nm. (c) CIE diagram associated with steady-state PL spectra in (b) as a function of temperature.

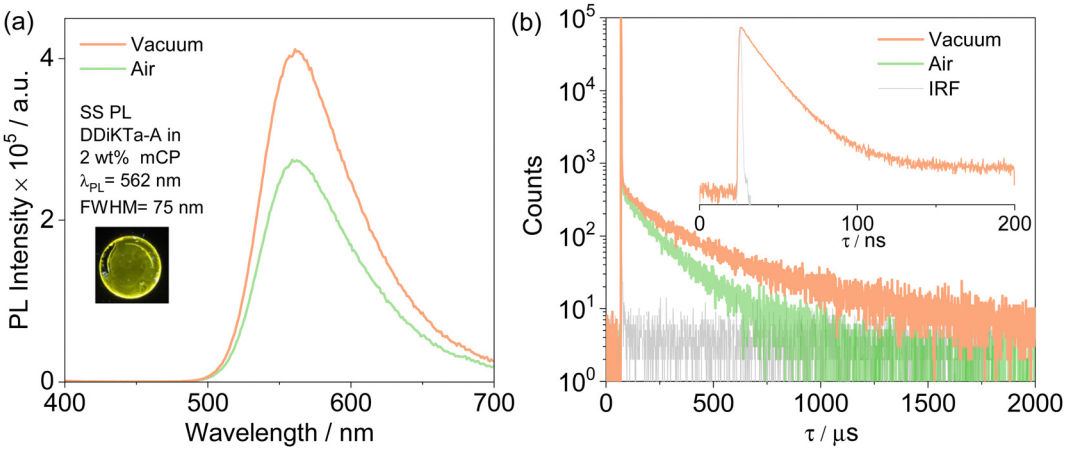

Fig. 5 (a) Steady-state PL spectra, λ_{exc} = 340 nm (Inset: photo of 1 wt% doped film of **DDiKTa-A** in mCP and irradiated with a UV torch, λ_{exc} = 365 nm.) and (b) time-resolved PL decays (inset is the PL decay of prompt component measured by TCSPC method), under vacuum and air of 2 wt% **DDiKTa-A** in mCP doped film, λ_{exc} = 375 nm.

Table 1 Photophysical data of **DDiKTa-A** and **DiKTa** in 2 wt% doped films in mCP

Emitters	Φ_{PL}/%[a]	λ_{PL}/nm[b]	FWHM/nm[c]	S_1/eV[d]	T_1/eV[e]	ΔE_{ST}/eV[f]	τ_p/ns[g]	τ_d/μs[g]	$k_{RISC}/10^4$ s^{-1}
DDiKTa-A	92	562	75	2.36	2.20	0.16	15.1	279	1.91
DiKTa[31]	46	467	46	2.75	2.55	0.20[25]	4.8	242	2.52

[a] The Φ_{PL} was measured using an integrating sphere under nitrogen (λ_{exc} = 340 nm). [b] Obtained at 298 K, λ_{exc} = 340 nm. [c] Full-width at half-maximum. [d] Obtained from the onset of the steady-state PL spectrum at 77 K. [e] Obtained from the onset of the delayed emission spectrum (1–10 ms) at 77 K (λ_{exc} = 340 nm). [f] $\Delta E_{ST} = E(S_1) - E(T_1)$. [g] Measured at 300 K under vacuum, λ_{exc} = 379 nm.

blue-shifts, ultimately reaching 566 nm at 123 K. This shift is attributed to the longer geometry relaxation time in frozen 2-MeTHF.[35] Importantly, this observation suggests that the red-shifted emission is a result of the sensitivity of the singlet state to the polarity of the environment, rather than aggregation during the cooling process.

To explore the potential of **DDiKTa-A** as an emitter in OLEDs, we turned our attention to assessing the photophysical properties in mCP thin films, as this host has a suitably high triplet energy (E_T = 3 eV)[39] to confine the excitons onto the emitter (Fig. 5). We first explored the dependence of both the SS PL and Φ_{PL} of **DDiKTa-A** on the doping concentration in mCP (Fig. S13, ESI†). Under N_2, the Φ_{PL} decreased from 92 to 74% upon increasing the doping concentration from 2 to 10 wt% in mCP, while the emission red-shifted from 562 to 588 nm, indicating that the emitter tends to aggregate and that these aggregates quench the emission. Therefore, using only the 2 wt% films, we next screened the properties in two other high triplet energy hosts, PPT and DPEPO (Fig. S14, ESI†). In both phosphine oxide-based hosts, the 2 wt% films emit at around 600 nm while the Φ_{PL} are 69 and 50%, respectively. The observed red-shifting of the emission from orange in mCP (λ_{PL} = 562 nm, FWHM = 75 nm) to red (λ_{PL} = 600 nm, FWHM = 102 nm) in these two hosts can be attributed to the increased stabilization of the LRCT state with increasing host polarity. Due to the high Φ_{PL} and narrower emission in the 2 wt% doped films in mCP, we carried out the subsequent photophysical studies using this film. The ΔE_{ST} of **DDiKTa-A** in this film is 0.16 eV (Fig. S15, ESI†), which is of similar magnitude to that measured in 2-MeTHF glass. The emission is quenched in the presence of air, dropping from a Φ_{PL} of 92 to 80%. There is the characteristic temperature dependence of the delayed emission that is indicative of TADF (Fig. S16, ESI†). The TR PL decay at RT shows multiexponential kinetics under vacuum, the average τ_P and τ_d are 15.1 ns and 279 μs, The kinetics rate constants for the 2 wt% doped films in mCP are collected in Table S2 (ESI†) and the k_{RISC} is 1.9 × 10^4 s^{-1} for **DDiKTa-A**, which is similar to that determined in 2 wt% doped film in mCP for **DiKTa** (k_{RISC} = 2.5 × 10^4 s^{-1}).[31] A summary of the photophysical properties of the 2 wt% doped films in mCP is provided in Table 1.

Device characterization

Vacuum-deposited OLEDs with **DDiKTa-A** were firstly fabricated with the device structure of: ITO/TAPC (35 nm)/TCTA (10 nm)/CzSi (10 nm)/*x* wt% emitter: mCP/(20 nm)/TmPyPB (40 nm)/LiF (1 nm)/Al (100 nm), where indium tin oxide (ITO) is the anode, 4,4′-cyclohexylidenebis[*N*,*N*-bis(4-methylphenyl) benzenamine] (TAPC) acts as the hole-transport layer. 9-(4-*tert*-butylphenyl)-3,6-bis(triphenylsilyl)-9*H*-carbazole (CzSi) is used to block excitons, 1,3,5-tri(*m*-pyridin-3-ylphenyl)benzene (TmPyPB) acts as the electron-transporting material, and LiF

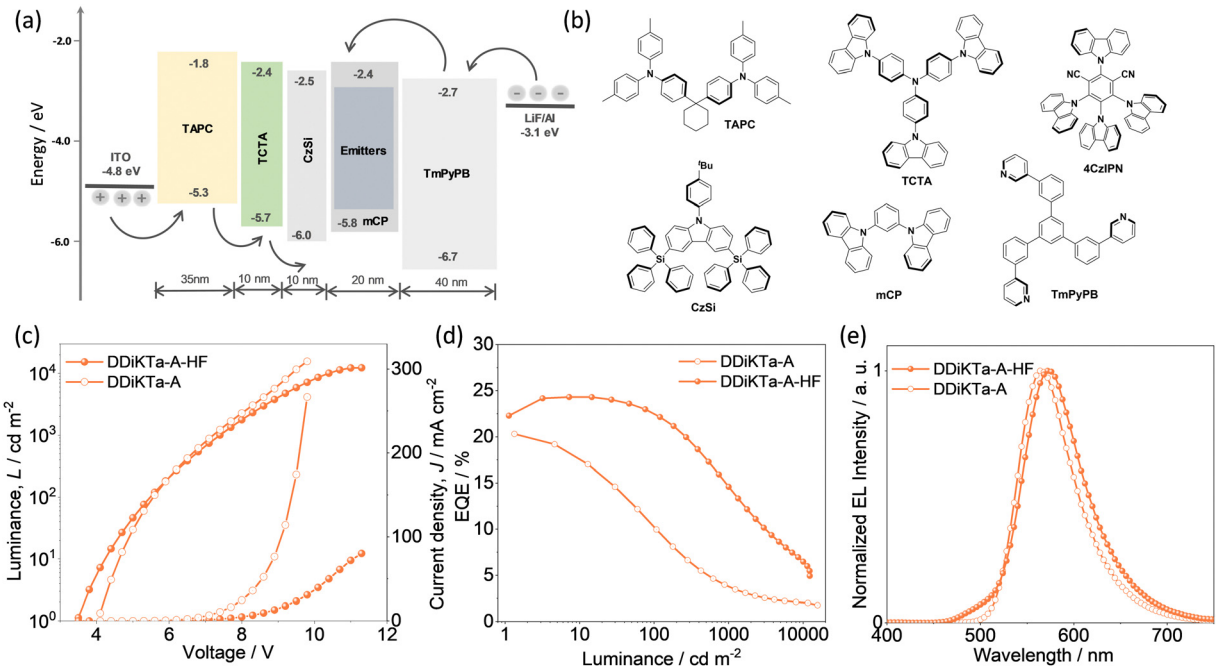

Fig. 6 a) Energy level diagram of materials employed in the devices. (b) Molecular structures of materials used in the devices. (c) Current density and luminance *versus* voltage characteristics for the devices. (d) External quantum efficiency *versus* luminance curves for the devices. (e) Electroluminescence spectra of the devices.

Table 2 Electroluminescence data

Emissive layer	V_{on}[a]/V	λ_{EL}/nm	FWHM[b]/nm	CIE (x, y)	L_{max}[c]/cd m^{-2}	EQE$_{max/100/1\,000}$[d]/%
DDiKTa-A/mCP	3.6	572	69	0.49, 0.50	12 390	20.3/13.2/3.9
DDiKTa-A/4CzIPN/mCP	3.5	574	75	0.48, 0.50	12 310	24.3/22.5/14.6
DiKTa/mCP[25]	3.0	465	39	0.14, 0.18	10 385	14.7/8.3/3.3

[a] Turn on voltage, recorded at 1 cd m^{-2}. [b] Full width at half-maximum of the electroluminescence spectrum. [c] Maximum luminance. [d] Maximum external quantum efficiency/EQE at 100 cd m^{-2}/EQE at 1 000 cd m^{-2}.

modifies the work function of the aluminum cathode. The device stacks and chemical structures of the materials are shown in Fig. 6b. The device performance is summarized in Fig. 6 and Fig. S17–S21 (ESI†) and Table 2.

Considering the small decrease in Φ_{PL} (from 92 to 73%) with an increase in doping concentration from 2 to 10 wt% in spin-coated mCP film, the emissive layers containing different doping concentrations of 2, 5, and 10 wt% in OLEDs were fabricated to assess how device performance is affected by doping concentration. The device with 5 wt% showed the best performance (Fig. S17, ESI†). The device emitted at an electroluminescence peak maximum, λ_{EL}, of 572 nm and was comparably broader to that observed in the PL spectrum (FWHM of 69 nm), Fig. 6e. The corresponding Commission Internationale de l'Éclairage (CIE) coordinates are (0.49, 0.50) The device showed an EQE$_{max}$ of 20.3%; however, there was a significant efficiency roll-off, with the EQE dropping to 13.2% at 100 cd m^{-2} (efficiency roll-off of 35%), which is attributed to the long τ_d of 279 μs of the emitter.

To address its rather inefficient exciton harvesting, we proceeded to fabricate a hyperfluorescence device (HF device), identifying 4CzIPN as a suitable assistant dopant. The emissive layer of the optimized HF device consisted of a 5 : 10 : 85 ratio for **DDiKTa-A**/4CzIPN/mCP. The photophysical properties are shown in Fig. S18–S19 (ESI†), and the spin-coated film emits at λ_{PL} at 577 nm, has a τ_p of 32 ns and τ_d of 149 μs and, importantly a Φ_{PL} of 98%. The corresponding k_{RISC} of this film is 5.47 × 10^4 s^{-1} (Table S2, ESI†). The HF device emitted at λ_{EL} of 574 nm (FWHM of 75 nm), which is a little broader than the device with only **DDiKTa-A**. The efficiency of the HF device was noticeably improved, with an EQE$_{max}$ of 24.3% and the device showed a significantly reduced efficiency roll-off of 7.4% and 40.0% at 100 and 1000 cd m^{-2} (EQE$_{100/1000}$ of 22.5 and 14.6%). This CIE coordinates of the HF device was (0.48, 0.50), representing one of only a handful of reported carbonyl-based orange/red MR-TADF OLEDs (Table S3 and Fig. S23, ESI†). Furthermore, it demonstrates a commendable EQE$_{max}$ of 24.3%, comparable to the literature device (with **QAD-mTDPA**) showing the highest EQE$_{max}$ of 26.3% for an orange/red carbonyl-based MR-TADF OLED,[40] and achieved the highest EQE$_{100}$ of 22.5% among carbonyl-based orange/red MR-TADF OLEDs (Fig. S23, ESI†).

Conclusions

In summary, we developed a yellow/orange MR-TADF emitter, **DDiKTa-A**, based on a design that bridges two **DiKTa** units *via* a central aniline. The synergistic combination of a compound containing *para*-N-π-N conjugation and two emissive luminophores resulted in a significantly red-shifted emission from blue (λ_{PL} = 453 nm) for **DiKTa** to yellow (λ_{PL} = 551 nm) for **DDiKTa-A** in toluene solution. In 2 wt% doped films in mCP, **DDiKTa-A** emits at 562 nm, with a high Φ_{PL} of 92% and a τ_d of 279 μs. Notably, in 2-MeTHF, the emission of **DDiKTa-A** displayed a spectral sensitivity to temperature over 123 to 298 K, reflecting temperature-dependent changes in the environment. The OLEDs with **DDiKTa-A** exhibited an EQE_{max} of 20.3% but that showed considerable efficiency roll-off, with an EQE_{100} of 13.2%. The device performance was markedly improved by employing a hyperfluorescence device stack with 4CzIPN as the assistant dopant, leading to a high EQE_{max} of 24.3% and a reduced efficiency roll-off with EQE_{100} of 22.5% and EQE_{1000} of 14.6% at λ_{EL} of 574 nm. This emitter design, where a central aniline bridges two MR-TADF units, provides a straightforward approach to developing MR-TADF compounds where the emission is significantly red-shifted to lower energy.

Data availability

The research data supporting this publication can be accessed at **https://doi.org/10.17630/7f97b17e-237f-400c-8bd4-1dfa093eedc4**.

Conflicts of interest

There are no conflicts to declare.

Acknowledgements

S. W. and J. X. W. thank the China Scholarship Council (201906250199, 202006250026) for support. Dianming Sun acknowledges support from the Royal Academy of Engineering Enterprise Fellowship (EF2122-13106). E. Z.-C. thanks the Engineering and Physical Sciences Research Council (EP/W015137/1, EP/W007517/1). X.-H. Z. acknowledges support by the National Natural Science Foundation of China (Grant No. 52130304, 51821002) and the Collaborative Innovation Center of Suzhou Nano Science & Technology.

References

1 S. Madayanad Suresh, D. Hall, D. Beljonne, Y. Olivier and E. Zysman-Colman, *Adv. Funct. Mater.*, 2020, **30**, 1908677.
2 R. K. Konidena and K. R. Naveen, *Adv. Photonics Res.*, 2022, **3**, 2200201.
3 T. Hatakeyama, K. Shiren, K. Nakajima, S. Nomura, S. Nakatsuka, K. Kinoshita, J. Ni, Y. Ono and T. Ikuta, *Adv. Mater.*, 2016, **28**, 2777–2781.
4 M. Y. Wong and E. Zysman-Colman, *Adv. Mater.*, 2017, **29**, 1605444.
5 Y. Tao, K. Yuan, T. Chen, P. Xu, H. Li, R. Chen, C. Zheng, L. Zhang and W. Huang, *Adv. Mater.*, 2014, **26**, 7931–7958.
6 H.-Z. Li, F.-M. Xie, Y.-Q. Li and J.-X. Tang, *J. Mater. Chem. C*, 2023, **11**, 6471–6511.
7 X.-C. Fan, K. Wang, Y.-Z. Shi, Y.-C. Cheng, Y.-T. Lee, J. Yu, X.-K. Chen, C. Adachi and X.-H. Zhang, *Nat. Photon.*, 2023, **17**, 280–285.
8 Y. Zhang, G. Li, L. Wang, T. Huang, J. Wei, G. Meng, X. Wang, X. Zeng, D. Zhang and L. Duan, *Angew. Chem., Int. Ed.*, 2022, **61**, e202202380.
9 J. Liu, Y. Zhu, T. Tsuboi, C. Deng, W. Lou, D. Wang, T. Liu and Q. Zhang, *Nat. Commun.*, 2022, **13**, 4876.
10 Y. Liu, X. Xiao, Z. Huang, D. Yang, D. Ma, J. Liu, B. Lei, Z. Bin and J. You, *Angew. Chem., Int. Ed.*, 2022, **61**, e202210210.
11 S. Uemura, S. Oda, M. Hayakawa, R. Kawasumi, N. Ikeda, Y.-T. Lee, C.-Y. Chan, Y. Tsuchiya, C. Adachi and T. Hatakeyama, *J. Am. Chem. Soc.*, 2023, **145**, 1505–1511.
12 H. L. Lee, W. J. Chung and J. Y. Lee, *Small*, 2020, **16**, 1907569.
13 S. Madayanad Suresh, L. Zhang, D. Hall, C. Si, G. Ricci, T. Matulaitis, A. M. Z. Slawin, S. Warriner, Y. Olivier, I. D. W. Samuel and E. Zysman-Colman, *Angew. Chem., Int. Ed.*, 2023, **62**, e202215522.
14 C.-Y. Chan, S. Madayanad Suresh, Y.-T. Lee, Y. Tsuchiya, T. Matulaitis, D. Hall, A. M. Z. Slawin, S. Warriner, D. Beljonne, Y. Olivier, C. Adachi and E. Zysman-Colman, *Chem. Commun.*, 2022, **58**, 9377–9380.
15 S. M. Suresh, L. Zhang, T. Matulaitis, D. Hall, C. Si, G. Ricci, A. M. Z. Slawin, S. Warriner, D. Beljonne, Y. Olivier, I. D. W. Samuel and E. Zysman-Colman, *Adv. Mater.*, 2023, **33**, 2300997.
16 M. Yang, I. S. Park and T. Yasuda, *J. Am. Chem. Soc.*, 2020, **142**, 19468–19472.
17 Y. Zhang, D. Zhang, T. Huang, A. J. Gillett, Y. Liu, D. Hu, L. Cui, Z. Bin, G. Li, J. Wei and L. Duan, *Angew. Chem., Int. Ed.*, 2021, **60**, 20498–20503.
18 Y. Zou, J. Hu, M. Yu, J. Miao, Z. Xie, Y. Qiu, X. Cao and C. Yang, *Adv. Mater.*, 2022, **34**, 2201442.
19 A. T. Gogoulis, R. Hojo, K. Bergmann and Z. M. Hudson, *Org. Lett.*, 2023, **25**, 7791–7795.
20 X. Cai, Y. Xu, Y. Pan, L. Li, Y. Pu, X. Zhuang, C. Li and Y. Wang, *Angew. Chem., Int. Ed.*, 2023, **62**, e202216473.
21 H. Chen, T. Fan, G. Zhao, D. Zhang, G. Li, W. Jiang, L. Duan and Y. Zhang, *Angew. Chem., Int. Ed.*, 2023, **62**, e202300934.
22 D. Sun, S. M. Suresh, D. Hall, M. Zhang, C. Si, D. B. Cordes, A. M. Z. Slawin, Y. Olivier, X. Zhang and E. Zysman-Colman, *Mater. Chem. Front.*, 2020, **4**, 2018–2022.
23 M. Yang, R. K. Konidena, S. Shikita and T. Yasuda, *J. Mater. Chem. C*, 2023, **11**, 917–922.
24 M. Wang, Z. Fu, R. Cheng, J. Du, T. Wu, Z. Bin, D. Wu, Y. Yang and J. Lan, *Chem. Commun.*, 2023, **59**, 5126–5129.
25 D. Hall, S. M. Suresh, P. L. dos Santos, E. Duda, S. Bagnich, A. Pershin, P. Rajamalli, D. B. Cordes, A. M. Z. Slawin,

D. Beljonne, A. Köhler, I. D. W. Samuel, Y. Olivier and E. Zysman-Colman, *Adv. Opt. Mater.*, 2020, **8**, 1901627.
26 Y. Yuan, X. Tang, X.-Y. Du, Y. Hu, Y.-J. Yu, Z.-Q. Jiang, L.-S. Liao and S.-T. Lee, *Adv. Opt. Mater.*, 2019, **7**, 1801536.
27 X. Li, Y.-Z. Shi, K. Wang, M. Zhang, C.-J. Zheng, D.-M. Sun, G.-L. Dai, X.-C. Fan, D.-Q. Wang, W. Liu, Y.-Q. Li, J. Yu, X.-M. Ou, C. Adachi and X.-H. Zhang, *ACS Appl. Mater. Interfaces*, 2019, **11**, 13472–13480.
28 Y. Xu, Z. Cheng, Z. Li, B. Liang, J. Wang, J. Wei, Z. Zhang and Y. Wang, *Adv. Opt. Mater.*, 2020, **8**, 1902142.
29 D. Hall, S. M. Suresh, P. L. dos Santos, E. Duda, S. Bagnich, A. Pershin, P. Rajamalli, D. B. Cordes, A. M. Z. Slawin, D. Beljonne, A. Köhler, I. D. W. Samuel, Y. Olivier and E. Zysman-Colman, *Adv. Opt. Mater.*, 2020, **8**, 1901627.
30 D. Hall, J. C. Sancho-García, A. Pershin, G. Ricci, D. Beljonne, E. Zysman-Colman and Y. Olivier, *J. Chem. Theory Comput.*, 2022, **18**, 4903–4918.
31 S. Wu, L. Zhang, J. Wang, A. Kumar Gupta, I. D. W. Samuel and E. Zysman-Colman, *Angew. Chem., Int. Ed.*, 2023, **62**, 202305182.
32 D. Sun, S. M. Suresh, D. Hall, M. Zhang, C. Si, D. B. Cordes, A. M. Z. Slawin, Y. Olivier, X. Zhang and E. Zysman-Colman, *Mater. Chem. Front.*, 2020, **4**, 2018–2022.
33 A. Pershin, D. Hall, V. Lemaur, J.-C. Sancho-Garcia, L. Muccioli, E. Zysman-Colman, D. Beljonne and Y. Olivier, *Nat. Commun.*, 2019, **10**, 597.
34 D. Hall, J. C. Sancho-García, A. Pershin, G. Ricci, D. Beljonne, E. Zysman-Colman and Y. Olivier, *J. Chem. Theory Comput.*, 2022, **18**, 4903–4918.
35 Z. Zhang, R. M. Edkins, J. Nitsch, K. Fucke, A. Steffen, L. E. Longobardi, D. W. Stephan, C. Lambert and T. B. Marder, *Chem. Sci.*, 2015, **6**, 308–321.
36 P. M. Kiefer and J. T. Hynes, *Isr. J. Chem.*, 2004, **44**, 171–184.
37 P. D. Zoon and A. M. Brouwer, *Photochem. Photobiol. Sci.*, 2009, **8**, 345–353.
38 R. R. Tan, X. Shen, L. Hu and F. S. Zhang, *Chin. Phys. B*, 2012, **21**, 086402.
39 S. A. Bagnich, A. Rudnick, P. Schroegel, P. Strohriegl and A. Köhler, *Philos. Trans. R. Soc., A*, 2015, **373**, 20130446.
40 F. Huang, K. Wang, Y. Z. Shi, X. C. Fan, X. Zhang, J. Yu, C. S. Lee and X. H. Zhang, *ACS Appl. Mater. Interfaces*, 2021, **13**, 36089–36097.

